



**HAL**  
open science

## Subsolar Al/Si and Mg/Si ratios of non-carbonaceous chondrites reveal planetesimal formation during early condensation in the protoplanetary disk

Morbidelli Alessandro, G. Libourel, H. Palme, S.A. Jacobson, D.C. Rubie

► **To cite this version:**

Morbidelli Alessandro, G. Libourel, H. Palme, S.A. Jacobson, D.C. Rubie. Subsolar Al/Si and Mg/Si ratios of non-carbonaceous chondrites reveal planetesimal formation during early condensation in the protoplanetary disk. *Earth and Planetary Science Letters*, 2020, 538, pp.116220. 10.1016/j.epsl.2020.116220 . hal-02996574

**HAL Id: hal-02996574**

**<https://hal.science/hal-02996574>**

Submitted on 20 May 2022

**HAL** is a multi-disciplinary open access archive for the deposit and dissemination of scientific research documents, whether they are published or not. The documents may come from teaching and research institutions in France or abroad, or from public or private research centers.

L'archive ouverte pluridisciplinaire **HAL**, est destinée au dépôt et à la diffusion de documents scientifiques de niveau recherche, publiés ou non, émanant des établissements d'enseignement et de recherche français ou étrangers, des laboratoires publics ou privés.



Distributed under a Creative Commons Attribution - NonCommercial 4.0 International License

1 **Subsolar Al/Si and Mg/Si ratios of non-carbonaceous chondrites**  
2 **reveal planetesimal formation during early condensation in the**  
3 **protoplanetary disk**

4 **A. Morbidelli<sup>(1)</sup>, G. Libourel<sup>(1)</sup>, H. Palme<sup>(2)</sup>, S. A. Jacobson<sup>(3)</sup> and D. C. Rubie<sup>(4)</sup>**

5 (1) Laboratoire Lagrange, UMR7293, Université de Nice Sophia-Antipolis, CNRS,  
6 Observatoire de la Côte d'Azur. Boulevard de l'Observatoire, 06304 Nice Cedex 4, France.

7 (Email: morby@oca.eu / Fax: +33-4-92003118)

8 (2) Senckenberg, world of biodiversity, Sektion Meteoritenforschung. Senckenberganlage 25,  
9 60325 Frankfurt am Main, Germany

10 (3) Northwestern University, Dept. of Earth and Planetary Sciences, Evanston, 60208  
11 Illinois

12 (4) Bayerisches Geoinstitut, University of Bayreuth, 95440, Bayreuth, Germany

13 Received \_\_\_\_\_; accepted \_\_\_\_\_

**ABSTRACT**

14

15

The Al/Si and Mg/Si ratios in non-carbonaceous chondrites are lower than the solar (i.e., CI-chondritic) values, in sharp contrast to the non-CI carbonaceous meteorites and the Earth, which are enriched in refractory elements and have Mg/Si ratios that are solar or larger. We show that the formation of a first generation of planetesimals during the condensation of refractory elements implies the subsequent formation of residual condensates with strongly sub-solar Al/Si and Mg/Si ratios. The mixing of residual condensates with different amounts of material with solar refractory/Si element ratios explains the Al/Si and Mg/Si values of non-carbonaceous chondrites. To match quantitatively the observed ratios, we find that the first-planetesimals should have accreted when the disk temperature was  $\sim 1,330$ – $1,400$  K depending on pressure and assuming a solar C/O ratio of the disk. We discuss how this model relates to our current understanding of disk evolution, grain dynamics, and planetesimal formation. We also extend the discussion to moderately volatile elements (e.g., Na), explaining how it may be possible that the depletion of these elements in non-carbonaceous chondrites is correlated with the depletion of refractory elements (e.g., Al). Extending the analysis to Cr, we find evidence for a higher than solar C/O ratio in the protosolar disk's gas when/where condensation from a fractionated gas occurred. Finally, we discuss the possibility that the supra-solar Al/Si and Mg/Si ratios of the Earth are due to the accretion of  $\sim 40\%$  of the mass of our planet from the first-generation of refractory-rich planetesimals.

## 1. Introduction

Carbonaceous chondrites (CCs), from CI to CM, CO and CV, show a progressive increase in Al/Si and Mg/Si ratios together with an increasing depletion in moderately volatile elements (e.g., Na) - see Fig. 1, table S1 and references therein. CI meteorites reflect the solar composition and the observed trend is interpreted as the consequence of an increasing abundance of minerals formed in high-temperature regions of the protoplanetary disk (e.g., CAIs: Hezel et al., 2008). The trend continues for the Earth, if the upper mantle Mg/Si and Al/Si ratios are valid for the bulk mantle, which is often assumed (e.g., Palme and O'Neill, 2014; Hyung et al., 2016), but there are also arguments against a chemically uniform mantle (e.g., Ballmer et al., 2013). There is also some discussion on the amount of Si in the core (Rubie et al., 2015). Thus, in Fig. 1 we report two values for the bulk Al/Si and Mg/Si ratios, computed assuming that the mantle is homogeneous (Hyung et al., 2016) but the core contains 0% or 7% Si by mass. This is intended to give a sense of the systematic uncertainty on the bulk composition ratios of the Earth. It remains clear, however, that the Earth is enriched in refractory elements and depleted in moderately volatile elements at least at the level of CO-CV meteorites.

Enstatite chondrites, rumuruti and ordinary chondrites (ECs, RCs and OCs hereafter, generically denoted NCCs for non-carbonaceous chondrites) surprisingly do not follow this trend, despite the fact that they should have formed in the relatively hot, inner solar system. Their Al/Si and Mg/Si ratios are sub-solar while they have only a small Na depletion compared to COs, CVs and the Earth (Fig. 1).

The strong difference in Al/Si and Mg/Si ratios between the Earth and ECs poses a conundrum. Most elements have the same ratios of stable isotopes (e.g., O-isotopes) in ECs and Earth, whereas other chondritic meteorites show significant differences. Small nucleosynthetic anomalies for ECs relative to Earth have been reported for Mo, Ru and Nd.

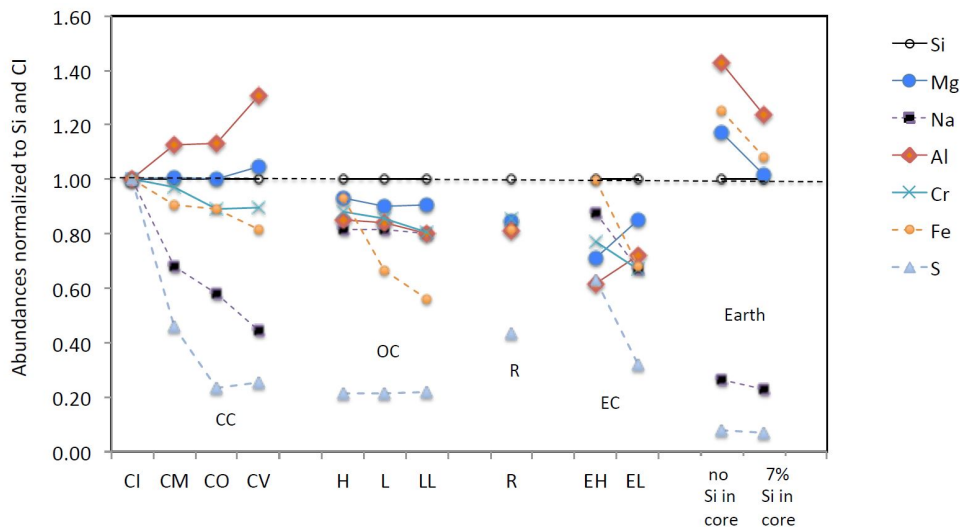


Fig. 1.— Abundances of Al, Mg, Fe, Cr, Na, S, relative to Si and normalized to the CI ratios for different chondrites and the Earth (data and references reported in table S1). For the bulk Earth (BE) two cases are given assuming 0 and 7wt% of Si in the core respectively. There is a clear difference in chemistry between the carbonaceous chondrites (CC) and the non-carbonaceous chondrites.

41 For this reason it is sometimes suggested that the Earth accreted mostly from enstatite  
 42 chondrites (see for instance Javoy, 1995; Lodders, 2000, Dauphas, 2017). But the large  
 43 differences in Al/Si and Mg/Si ratios between the Earth and ECs seem to preclude this  
 44 possibility, although some solutions have been proposed (e.g., incongruent vaporization of  
 45 enstatite: see Mysen and Kushiro, 1988). Dauphas (2017) postulated that the precursors of  
 46 the Earth had the same isotopic composition as ECs but a different element composition.

47 It has been proposed that the sub-solar Al/Si and Mg/Si ratios in the NCCs are due  
 48 to the loss of a refractory-rich component from a disk with an original solar composition  
 49 (see Larimer, 1979; see also Alexander, 2019 and references therein). It has also been  
 50 suggested that this refractory component was accreted by the Earth, thus explaining its  
 51 enrichment in refractory elements. For instance, to explain the Mg-enrichment of the Earth,  
 52 Dauphas et al. (2015) suggested that the ECs were depleted in a forsterite condensate and  
 53 are complementary to the forsterite enriched Earth. This possibility has been explicitly  
 54 excluded by Alexander (2019), for the reasons discussed in Sect. 5. An alternative

55 explanation for the relative deficiency of Si and Mg in the Earth is the evaporation from the  
56 molten surface of the protoplanetary embryos that made our planet (Pringle et al., 2014;  
57 Mysen and Kushiro, 1988; Hin et al., 2017; Young et al., 2019). However, the sub-solar  
58 Al/Si and Mg/Si ratios of the NCCs cannot be explained by evaporation models because Si  
59 should be lost preferentially relative to Mg and Al.

60 In this paper, we revisit the idea of the sequestration of a refractory component from  
61 the protoplanetary disk in order to explain the depletion of refractory elements in the  
62 NCCs. In section 2, we discuss how a refractory-rich component could be sequestered, in  
63 the framework of modern models of disk evolution and planetesimal formation. In section 3,  
64 we determine the temperature at which this refractory-rich component should have been  
65 isolated from the condensation sequence in order to explain the Al/Si and Mg/Si of the  
66 NCCs. In section 4, we extend our considerations to other elements: Fe, Na, Cr and S.  
67 In section 5, we show that the enrichment in refractory elements of the Earth can be  
68 explained, within uncertainties, by the addition of the refractory component removed from  
69 the NCCs. We discuss how the issues that led Alexander (2019) to exclude this possibility  
70 can be solved, so that this possibility remains the most viable one. Section 6 summarizes  
71 the results and highlights the predictions of the properties of the protoplanetary disk that  
72 our results imply, that will need to be validated by future models of disk’s formation and  
73 evolution.

## 74 **2. An astrophysical scenario for the sequestration of refractory material**

75 As often assumed, we consider that the inner disk was initially very hot, so all material  
76 was in a gaseous form, including refractory elements. As the disk was rapidly cooling,  
77 various species started to condense in sequence, from the most refractory to the more  
78 volatile. This is typical of equilibrium condensation where, with declining temperature,

79 some earlier condensed species are destroyed to form new ones, in addition to condensing  
80 new species.

81 However, it is unlikely that this process continued undisturbed to low temperatures.  
82 When enough solid grains condensed, but well before the completion of the whole sequence,  
83 the ionization level of the gas was strongly reduced by the now present dust and the  
84 magneto-rotational instability (MRI) generating turbulence in the midplane of the disk  
85 was quenched (Desch and Turner, 2015). Because the disk had a radial temperature  
86 gradient, this did not happen everywhere at the same time. The innermost part of the disk,  
87 hot enough to contain only small amounts of dust, remained MRI-active while the outer  
88 part located beyond a threshold distance corresponding to some temperature  $T_{MRI}$  was  
89 MRI-inactive; the boundary between the two parts moved sunwards as the disk cooled with  
90 time. The value of  $T_{MRI}$  is not known precisely. In this work, we will consider it as a free  
91 parameter and we discuss its best-fit value in section 3.1.

92 The transition from a MRI-active to a MRI-inactive region of the disk should  
93 correspond to a transition in gas density. The surface density of gas has to be larger in the  
94 MRI-inactive region for the conservation of mass flux:  $F_M = 2\pi r \Sigma v_r$ , where  $F_M$  is the mass  
95 flux,  $r$  is the distance from the star,  $\Sigma$  is the surface density of gas and  $v_r$  its radial velocity.  
96 In fact,  $v_r = -3/2(\nu/r)$  where  $\nu$  is the gas viscosity, so there is an anti-correlation between  
97  $\Sigma$  and  $\nu$ , the latter being much larger in the MRI-active region of the disk. This steep  
98 density gradient, creating a pressure maximum, acts as a barrier to the inward radial drift  
99 of dust due to gas drag. Thus, at the boundary between the MRI-active and MRI-inactive  
100 parts of the disk we expect to find not just the locally-condensed grains corresponding to  
101 that temperature, but also grains that condensed earlier and farther away and whose radial  
102 migration was stopped at this boundary (Flock et al., 2017). Incidentally, these migrated  
103 grains trapped at  $T_{MRI}$  would evolve to acquire the same chemistry as those condensed

104 locally at  $T_{MRI}$ . Hence, the dust/gas ratio at  $T_{MRI}$  can become much larger with time than  
 105 the value due solely to the locally-condensed grains.

106 This accumulation of dust (Flock et al., 2017) should have triggered rapid planetesimal  
 107 formation via the streaming instability (Youdin and Goodman, 2005; Johansen and Youdin,  
 108 2007). It is indeed known that this instability is triggered when the solid/gas mass ratio  
 109 exceeds by 3-4 times the value corresponding to the condensation of dust from a gas of  
 110 solar composition (the exact value depending on particle size; Yang et al., 2017). With  
 111 the formation of planetesimals, the already condensed material stops participating in the  
 112 gas-solid equilibrium chemistry because it becomes locked-up in large objects instead of  
 113 small grains.

114 Consequently, at the temperature  $T_{MRI}$  there should have been a bifurcation in the  
 115 chemistry of the disk due to the fractionation of solids from gas. Below  $T_{MRI}$ , condensation  
 116 could form new solid species only from the *residual* gas. Consequently, the first generation of  
 117 planetesimals should have been refractory-rich, with strongly supra-solar Al/Si and Mg/Si  
 118 ratios, whereas the second generation of solids condensed from the residual gas (denoted  
 119 “residual condensates” hereafter for brevity) should have been extremely refractory-poor,  
 120 with strongly sub-solar Al/Si and Mg/Si ratios.

121 This sequence of events and the roles of residual condensates, first planetesimals and  
 122 solar-composition material in making the NCCs and the Earth are depicted in Fig. 2 and  
 123 are described in more details in the subsequent sections.

### 124 **3. Determining the temperature of sequestration of refractory material**

125 To determine  $T_{MRI}$ , the temperature of sequestration of the first condensates in  
 126 planetesimals, we follow the condensation sequence from a gas of solar composition to track

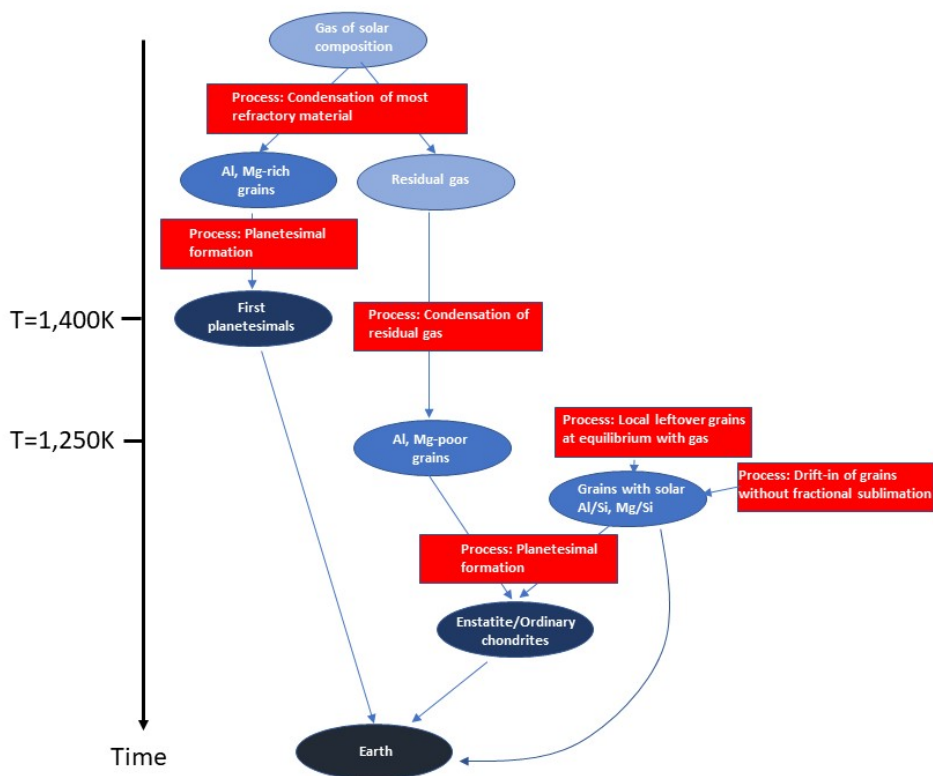


Fig. 2.— A flow-chart of the scenario explored in this paper. The vertical axis represents the evolution of time, from top to bottom, during which the temperature decreases. The blue ellipses show the material available (light blue for gas then -with increasing intensity of the color- grains, planetesimals and the Earth) and the red rectangles show the transformation processes. For simplicity, we do not track volatiles condensing below 1,250K, nor H and He. See also Supplementary Fig. 3 for a more comprehensive (but complicated!) sketch of the evolution of gas and solids in the disk as a function of distance, time and declining temperature.

127 the species condensed and the chemical composition of the residual gas as a function of  
 128 temperature (sect. 3.1). Then, we use these data to determine the temperature that fits  
 129 best the observed Al/Si and Mg/Si ratios of the NCCs (sect. 3.2).

130

### 3.1. Condensation sequence

131

We have computed a condensation sequence, during the cooling of the disk at the  
 132 mid-plane of the Solar Nebula, starting from 2,000 K and assuming a total pressure of  $10^{-3}$   
 133 bar and a solar C/O ratio. Some results for different pressures and C/O ratios are also

134 reported below. These calculations describe the equilibrium distribution of the elements  
135 and their compounds between coexisting phases (solids, liquid, vapor) in a closed chemical  
136 system with vapor always present upon cooling. We have used for this proof of concept a  
137 simplified solar gas composition taken from Ebel and Grossman (2000) composed of the  
138 most abundant elements of the solar photosphere: H, C, O, Mg, Si, Fe, Ni, Al, Ca, Ti, Cr,  
139 S and Na.

140 The equilibrium condensation sequence of this simplified solar gas has been calculated  
141 using the FactSage software package (Bale et al., 2016) by means of a general Gibbs free  
142 energy minimization method (Eriksson and Hack, 1990). The thermodynamic data for each  
143 compound are taken from the database provided by the FactSage package. The potential  
144 number of species that can be formed from the combination of the 13 elements considered in  
145 this system is over 450, comprising 150 gases and 320 pure solid phases (see tables S2, S3).  
146 For this proof of concept, condensation calculations have been performed in steps of 10 K,  
147 allowing only pure solid phases to condense, no solid solutions (see below).

148 Figure 3 shows the fractions of the condensable mass and of Al, Mg, and Si that have  
149 condensed as a function of temperature, respectively. The comparison with published  
150 results on the condensation of a gas of solar composition (Yoneda and Grossman, 1995; Ebel  
151 and Grossman, 2000; Ebel 2006) shows a good agreement in terms of both the computed  
152 condensation temperatures and the sequence of appearance of solid phases upon cooling  
153 (Fig. 3a), despite the use of only pure solid phases.

154 As is well known, corundum starts to condense first at a temperature of  $\sim 1,775$  K  
155 at the pressure considered here ( $10^{-3}$  bar). It is followed by calcium aluminates (hibonite,  
156 perovskite, grossite and melilite), which set the Al contents of the first condensates to be  
157 very high. Magnesium and Si start to condense later, almost simultaneously at  $T \sim 1,600$  K  
158 with the onset of the condensation of melilite. Both Mg and Si contents increase as cooling

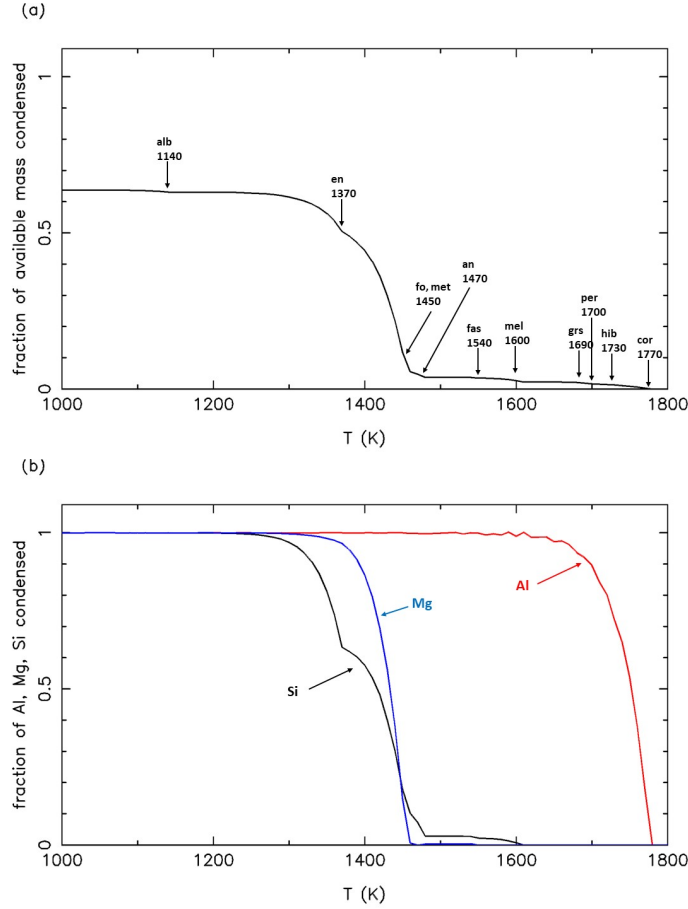


Fig. 3.— a) Fraction of the total condensable mass from a cooling vapor of solar composition (i.e., CI composition, including volatiles) at  $P_{tot} = 10^{-3}$  bar. Arrows indicate the onset of pure solid phase condensation together with their temperature. Abbreviations, cor: corundum ( $\text{Al}_2\text{O}_3$ ); hib: hibonite ( $\text{CaAl}_{12}\text{O}_{19}$ ); per : perovskite ( $\text{CaTiO}_3$ ); grs: grossite ( $\text{CaAl}_4\text{O}_7$ ); mel: mellitite ( $\text{Ca}_2\text{Al}_2\text{SiO}_7$ ); fas: Aluminous-rich clinopyroxene ( $\text{CaAl}_2\text{SiO}_6$  – mimicking fassaite-like Fe poor, Ca, Al, Ti pyroxene); sp: spinel ( $\text{MgAl}_2\text{O}_4$ ); met: Fe-Ni metal; fo: forsterite ( $\text{Mg}_2\text{SiO}_4$ ); an: anorthite ( $\text{CaAl}_2\text{Si}_2\text{O}_8$ ); en: enstatite ( $\text{MgSiO}_3$ ); alb: albite ( $\text{NaAlSi}_3\text{O}_8$ ). b) Fractions of available Al, Mg and Si condensed as a function of temperature. Note that Al/Si and Mg/Si ratios of condensates become solar at a temperature of  $\sim 1,250\text{K}$ . Note also that the Al/Mg ratio becomes solar at larger temperature than the Al/Si ratio.

159 proceeds in response to condensation of fassaite and spinel at lower temperature. Initially,  
 160 Si exceeds Mg in terms of fraction condensed but then, at  $1,250\text{ K} < T < 1,450\text{ K}$ , Mg  
 161 exceeds Si because of the condensation of forsterite ( $\text{Mg}_2\text{SiO}_4$ ), the first phase to remove  
 162 major fractions of Si and Mg from the gas. Further cooling of the solar gas promotes the  
 163 condensation of enstatite ( $\sim 1,370\text{ K}$ ) and leads to the subsequent increase in Si of the  
 164 solid. By the time the temperature has decreased to  $\sim 1,250\text{ K}$ , all available Al, Mg and

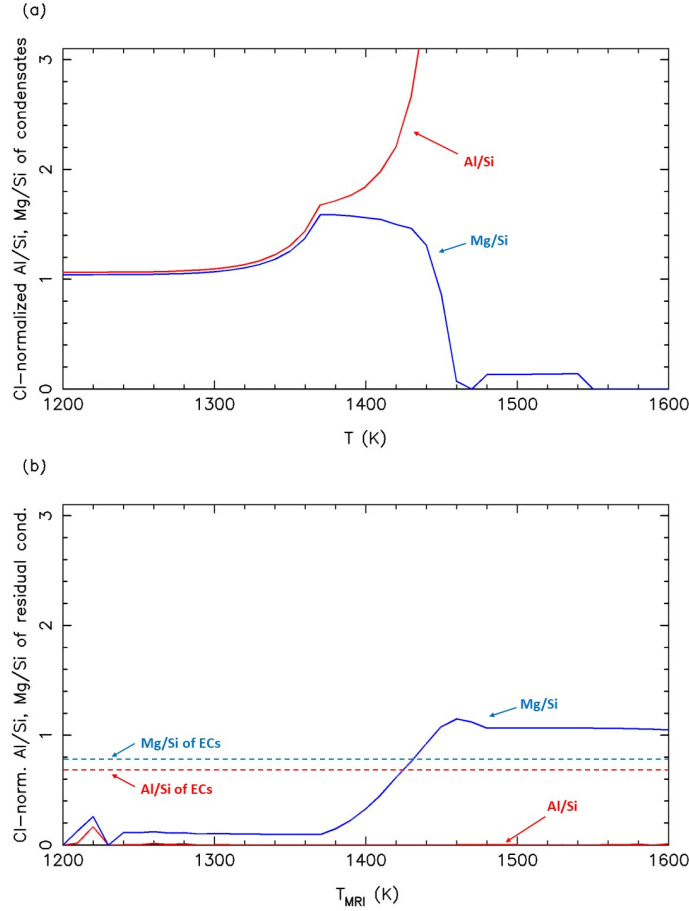


Fig. 4.— Top panel: the solid curves show the Al/Si (red) and Mg/Si (blue) ratios (normalized to CI values) of the condensed material as a function of gas temperature. The arrow indicates that the Al/Si ratio increases above the upper limit of the plot for  $T > 1,430$ K. Bottom panel: the same but for the residual condensates, assuming that all the early condensed material has been sequestered in planetesimals at the temperature  $T_{MRI}$ . The horizontal lines show the mean Al/Si and Mg/Si ratios for ECs.

165 Si atoms have condensed, which implies that the solar composition in terms of Al/Si and  
 166 Mg/Si is achieved at this temperature.

167 The top panel of Fig. 4 shows the resulting Al/Si (red) and Mg/Si ratios (blue) as a  
 168 function of temperature, normalized to the respective ratios in CI meteorites (i.e., the solar  
 169 composition ratios). The Al/Si ratio drops monotonically with decreasing temperature and  
 170 reaches the solar ratio (i.e., one when normalized) at  $T \sim 1,250$  K. The Mg/Si ratio instead  
 171 starts sub-solar but then becomes supra-solar for  $1,250 \text{ K} < T < 1,450 \text{ K}$ , with the bump

172 due to the condensation of forsterite.

173 If condensates are isolated from the gas at a temperature  $T_{MRI}$ , they maintain the  
 174 composition of the solids condensed at that temperature; thus, their Al/Si and Mg/Si  
 175 ratios are those shown in Fig. 4a at  $T = T_{MRI}$ . Strictly speaking, isolation occurs when  
 176 condensates grow big enough to prevent further gas-solid exchanges. For example, given  
 177 a diffusion coefficient of about  $10^{-16}\text{m}^2/\text{s}$  at 1,400 K for Fe-Mg interdiffusion in olivine  
 178 (Holzapfel et al., 2003), a mm-size grain would equilibrate in approximately 300 y and a  
 179 cm-size grain in 30,000 y. However, according to aggregation experiments it is likely that  
 180 most grains are sub-mm in size (Güttler et al., 2010). Thus the most effective way to isolate  
 181 solid material from exchange reactions with the gas is to incorporate it into macroscopic  
 182 planetesimals, as explained in the previous section.

183 Consider now the possibility that at some temperature  $T_{MRI}$  the condensed solids are  
 184 sequestered in planetesimals. Then, with further decreasing temperature, new solids will  
 185 condense from the residual gas. The bottom panel of Fig. 4 shows the Al/Si and Mg/Si  
 186 ratios of these residual condensates as a function of  $T_{MRI}$ . They are completely different  
 187 from those of the first condensates. The Al/Si ratio of the residual condensates is strongly  
 188 sub-solar (essentially zero below 1600 K, when all Al is condensed) and the Mg/Si ratio  
 189 is also sub-solar for  $T_{MRI} < 1,450$  K. Figure 4b shows, for comparison, the Al/Si and  
 190 Mg/Si ratios of ECs. Note that at no value of  $T_{MRI}$  do the residual condensates have  
 191 simultaneously both the Al/Si and Mg/Si ratios of these chondrites.

### 192 **3.2. Making non-carbonaceous chondrites**

193 It is dynamically unlikely and chemically impossible that the NCCs formed solely from  
 194 residual condensates. A fraction of the first condensed grains may have been small enough

195 to avoid piling up at  $T_{MRI}$ , thus remaining at equilibrium with the cooling gas. These  
 196 grains would have eventually acquired a solar composition in terms of concentrations of Al,  
 197 Mg and Si and -possibly also- moderately volatile elements. In addition, other grains with  
 198 solar elemental composition may have arrived from farther out in the disk. We stress that  
 199 these grains did not necessarily have the CI content of water and of other highly volatile  
 200 components, condensible only at low temperature<sup>1</sup>. Likewise, the isotopic properties of this  
 201 material are not necessarily the same as for CI meteorites. Thus, hereafter when using the  
 202 term "solar-composition" we simply refer to material characterized by solar abundances  
 203 of refractory and moderately volatile elements. We postulate that the NCCs formed as  
 204 a second generation of planetesimals from a mixture of these solar-composition grains  
 205 and residual condensates, so that they appear as if a refractory-rich component had been  
 206 partially subtracted, as the data suggest.

207 Thus, for each temperature  $T_{MRI}$  we compute the relative amount of solar-composition  
 208 material  $M_{Sol}$  that has to be mixed with the residual condensates to reproduce the Al/Si  
 209 and/or the Mg/Si ratio of the NCCs (Fig. 5).  $M_{Sol}$  is computed from the two equations:

$$\begin{aligned}
 R^{NCC} &= \frac{f_{Al,Mg}^{res} M_{res} + \tilde{f}_{Al,Mg}^{CI} M_{Sol}}{f_{Si}^{res} M_{res} + \tilde{f}_{Si}^{CI} M_{Sol}} \\
 1 &= M_{res} + M_{Sol}
 \end{aligned}
 \tag{1}$$

210 where  $R^{NCC}$  is the Al/Si or the Mg/Si weight ratio in the considered NCCs (ECs, RCs  
 211 or OCs);  $f_{Al,Mg}^{res}$  and  $f_{Si}^{res}$  are the concentrations by mass of Al, Mg and Si in residual  
 212 condensates (all these quantities depend on  $T_{MRI}$  and are shown in Fig. S1), whose total

---

<sup>1</sup>As we will see below, 60–90% of solar-composition material is required in the NCCs and the Earth. If the solar-composition material had been real CI material, both these chondrites and the Earth would be rich in water and other volatile elements of comparable volatility, which is not the case.

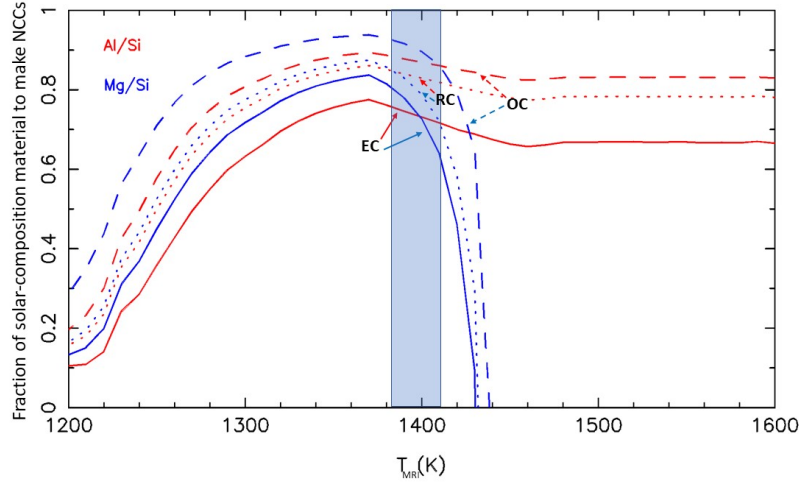


Fig. 5.— The fraction of solar-composition material that needs to be mixed with residual condensates to reproduce the Al/Si (red) and Mg/Si (blue) ratios of ECs (solid), OCs (dashed) and RCs (dotted), as a function of the temperature of formation of the first planetesimals,  $T_{MRI}$ . For ECs and OCs we use the mean of the ratios of the various sub-classes: Al/Si=0.67 and Mg/Si=0.78 and Al/Si=0.83 and Mg/Si=0.91 respectively, relative to CI ratios. The vertical band shows the range of values of  $T_{MRI}$  that satisfy the considered elemental ratios of all the NCCs types: 1,385–1,410 K.

213 mass is  $M_{res}$ ;  $\tilde{f}_{Al,Mg}^{CI}$  and  $\tilde{f}_{Si}^{CI}$  are 1.66 times the concentrations of Al, Mg and Si in CI  
 214 meteorites (see table S1 for element fraction in meteorites). The factor 1.66 takes into  
 215 account the lack of volatiles (e.g., water) in the solar-composition material that we consider  
 216 compared to CI meteorites, which reduces their total mass to 60%.

217 Obviously, for each meteorite class the concordia situation occurs at the intersection  
 218 between the two solutions, when both the Al/Si and Mg/Si ratios are reproduced for the  
 219 same combination of  $T_{MRI}$  and  $M_{Sol}$ . Note that the solutions for  $T_{MRI}$  are very similar  
 220 (1,385–1,405 K) for all the NCC classes. This means that the residual condensate material  
 221 (or, equivalently, the subtracted refractory component) is the same for these classes of  
 222 meteorites and that the different bulk chemical compositions of the ECs and OCs are  
 223 mostly due to different mixing proportions with the solar-composition material. Notice that  
 224 the relative mass of solar-composition material exceeds in all cases the fraction of matrix in  
 225 these meteorites. This means that the formation of chondrules and matrix occurred after

226 mixing solar-composition material and residual condensates. Hence, it does not contradict  
227 our model that the RCs are intermediate between ECs and OCs in terms of proportion of  
228 solar-composition material even if they have the largest proportion of matrix.

229 The elemental and the mineralogical compositions of the refractory material sequestered  
230 at 1,400 K are shown in the top panels of Fig. 6. We have repeated the calculation for  
231 a pressure of  $10^{-4}$  bar. Conceptually the results are the same, but all condensation  
232 temperatures shift to lower values;  $T_{MRI}$  is found to be in the range 1,310–1,330 K.

#### 233 4. Other elements

234 Now that  $T_{MRI}$  is determined, we can check the consistency of the model with other  
235 elements with different condensation temperatures.

236 We start our analysis with a moderate refractory element like Fe. For  $P = 10^{-3}$  bar,  
237 the residual condensates would have a sub-solar Fe/Si ratio (Fig. S1). However, for  
238  $P = 10^{-4}$  bar Fe is less refractory and the Fe/Si ratio at  $T_{MRI}$  is basically unfractionated.  
239 The amount of Fe varies widely within the ECs and OCs, from EH to EL and H to LL.  
240 These changes cannot be explained by our simple model here. They may require different  
241 oxidation conditions, in the disk, during chondrule formation (Larimer, 1979; Alexander,  
242 2019). We notice that because Fe tends to be present in meteorites as distinct metal blebs,  
243 Fe enrichment and depletion may also be due to size-sorting effects during the streaming  
244 instability.

245 Notice that in the top panels of Fig. 6 Ni does not appear. This is an artifact of our  
246 calculation scheme since only pure Fe and pure Ni metal phases (and not the single FeNi  
247 solid solution) have been taken into account. Thus, the Ni/Fe ratios in both the first and  
248 the residual condensates are not realistic.

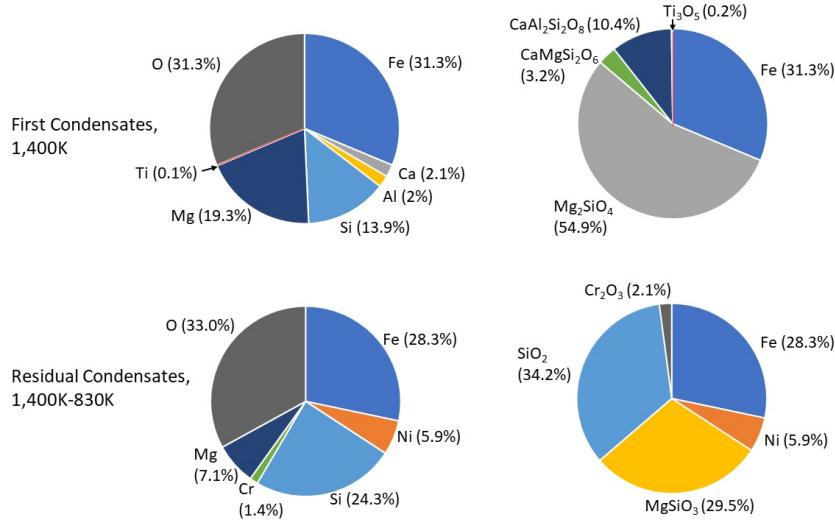


Fig. 6.— The elemental (left pie-charts) and mineralogical (right pie-charts) weight fractions for the first condensates at 1,400K (top) and residual condensates down to 830K (bottom).

249 Sodium is a more interesting case, because in the NCCs, with the exception of the  
 250 EH meteorites, it shows a striking correlation with Al (see Fig. 1). The same is true for  
 251 the other alkali elements (Alexander, 2019). According to our model, when the refractory  
 252 material is sequestered at 1,400 K, Na has not yet condensed, so the Na-Al correlation is  
 253 not expected.

254 However, as pointed out by Barshay and Lewis (1976), the sequestration of refractory  
 255 elements prevents their further reaction with the gas at lower temperatures, making Na  
 256 less able to condense, i.e., more volatile. For instance, in an equilibrium condensation  
 257 sequence, at  $P = 10^{-3}$  bar, the condensation of Na would start by forming NaAlSi<sub>3</sub>O<sub>8</sub>  
 258 (albite) at 1,150 K. But as Al has been removed from the gas, this mineral cannot form.  
 259 The first refractory-element-free condensate that Na can form is Na<sub>2</sub>S (Fegley and Lewis,  
 260 1980), which starts to condense below 830 K at  $P = 10^{-3}$  bar. Thus, if gas condensation  
 261 “ends” before this temperature is reached the residual condensates do not contain Na and  
 262 the final depletion in Na in the ECs and OCs correlates perfectly with the depletion in Al,  
 263 because both Na and Al are acquired only from the solar-composition component of these

264 meteorites.

265 We stress that it is natural that the condensation sequence ends when there is still gas  
 266 left in the system. In fact, condensation requires cooling the gas but, although the disk  
 267 cools over time at each location, parcels of gas are also radially transported towards the  
 268 star. Thus, there is a competition between heating of gas due to its inward radial drift and  
 269 secular cooling of the disk. Morbidelli et al. (2016) showed that a viscously evolving disk  
 270 transitions from condensing (cooling) gas parcels to inwardly drifting (heating) parcels after  
 271 half a viscous timescale ( $r^2/\nu$ ), which is a small fraction of the disk’s lifetime. In the disk  
 272 model of Bitsch et al. (2015) this happens at 1 AU at  $t \sim 10^4$  y, when the stellar accretion  
 273 rate is  $10^{-6}M_{\oplus}/y$ , before the temperature has reached  $\sim 800$  K. Assuming this is the case,  
 274 we show in the bottom row of Fig. 6 the elemental and the mineralogical compositions of  
 275 the residual condensates.

276 The case of Cr is more difficult. Still for our nominal case of  $P = 10^{-3}$  bar 50% of Cr  
 277 condenses at 1,300K, too close to  $T_{MRI}$  to invoke the premature end of the condensation  
 278 sequence, but not high enough to remove most of the Cr with the first condensates. Thus,  
 279 we should expect that the residual condensates were enriched in Cr and that the NCCs  
 280 have Cr/Si higher than the CI value. Instead, the depletion of Cr correlates with that of  
 281 Al (Alexander, 2019). Accounting for the solubility of Cr in Fe-metal and olivine allows  
 282 for the removal of  $\sim 50\%$  of the Cr with the first condensates, but  $\sim 50\%$  of Si is also  
 283 removed, so that the residual condensates should be at best un-fractionated in Cr/Si, which  
 284 is insufficient to explain the observed Al-Cr correlation. However, we find that if the C/O  
 285 ratio of the gas is increased to 0.9,  $T_{MRI}$  decreases to 1,280K (because the condensation  
 286 temperatures of Al, Mg and Si decrease), so that nearly 100% of Cr is bound in the first  
 287 condensates if one accounts for its solubility in iron and olivine. Thus a  $C/O \geq 0.9$  enables  
 288 the Cr-Al correlation in the NCCs to be explained. The same is true at lower pressure.

289 A similar C/O ratio has been invoked by several authors (e.g., Lodders and Fegley, 1993)  
 290 as the sole way to explain various properties of enstatite chondrites. It is interesting that  
 291 from a completely different approach we also reach this conclusion, with the difference that  
 292 in our model the high C/O ratio affected the formation of residual condensates that are a  
 293 component of all the NCCs, not just of the ECs (although more prominent in ECs). The  
 294 equivalent of Fig. 6, except for C/O=0.9, is given in Fig. S4.

295 Sulfur is more volatile than Na in a gas with solar C/O. But it starts to behave as a  
 296 refractory element for C/O > 0.9, when oldhmite (CaS) begins to condense. For C/O = 1.2,  
 297 40% of S is condensed at  $T_{MRI}$  (=1,130 K for  $P = 10^{-3}$  bar). No S condenses from the  
 298 residual gas before Na. Thus, S and Na depletions should correlate in the NCCs, but such  
 299 a correlation is not observed. Sulfur is mostly found in the matrix and high concentrations  
 300 of S are only observed in EC chondrules. Remembering that the mixing between residual  
 301 condensates and solar-composition material should be done at the level of chondrule  
 302 precursors this observation suggests that, for some reason, S was lost in the formation of  
 303 OCs and RCs chondrules, but not Na (Alexander et al., 2008).

## 304 5. The Earth

305 If the first-formed planetesimals had accreted with each other and possibly with  
 306 additional solar-composition material, they would have formed a planet enriched in  
 307 refractory elements. It is therefore important to check whether this scenario could explain  
 308 the supra-solar Al/Si and Mg/Si ratios of the Earth.

309 For simplicity we consider our nominal case of  $P = 10^{-3}$  bar and a solar C/O ratio.  
 310 We assume that the composition of the first-formed planetesimals is that obtained from the  
 311 equilibrium condensation at  $T_{MRI} = 1,400$ K (Fig. 6, top - see also Fig. S2) and use eq. (1)

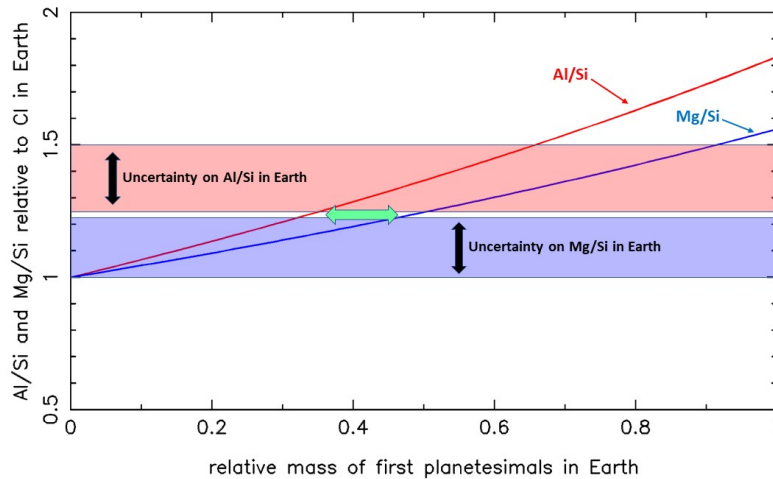


Fig. 7.— The Al/Si (red) and Mg/Si (blue) ratios as a function of the mass fraction of first, refractory rich planetesimals contributing to the Earth, the rest being accreted from solar-composition material. The horizontal colored bands show the estimated bulk terrestrial Mg/Si and Al/Si ratios and their uncertainties. These are reproduced if the Earth comprises 35-45% by mass of first planetesimals.

312 again. The Al/Si and Mg/Si ratios of the Earth increase as the relative mass fraction of  
 313 these planetesimals incorporated in the planet increases (the rest of Earth’s mass having a  
 314 solar composition) and we find that ratios consistent with the observed values within their  
 315 broad uncertainties can be obtained for a mass fraction of about 35-45% (Fig. 7).<sup>2</sup>

316 Alexander (2019) explicitly excluded the possibility that the refractory material missing  
 317 from the NCCs (i.e., our first-formed planetesimals) has been accreted by the Earth. His  
 318 conclusion is motivated by three arguments, which we review and discuss here.

319 First, he pointed out that the addition to solar-composition material of the refractory

---

<sup>2</sup>We note that combining first planetesimals with ECs would lead to equivalent results. In fact, the combination of first-condensed material with its complement of residual condensates gives by definition material with a solar bulk composition. Thus, the  $x$ -axis of Fig. 7 can be simply interpreted as the excess of first-condensed material in the Earth, whatever the combination of material that is envisioned.

320 material missing from the NCCs does not fit well the Earth’s composition. This is visible  
321 also in Fig. 7 because the Al/Si and Mg/Si ratios can be simultaneously reproduced only  
322 at the opposite extremes of their error bars. If the uncertainties on these ratios are entirely  
323 due to the amount of Si incorporated in the terrestrial core, they are not independent.  
324 So, in this case one cannot claim success if one ratio is reproduced at the high-end of its  
325 uncertainty limit and the other at its low-end. However, Young et al. (2019) argued that  
326 the Earth or its precursors lost by evaporation about 12% of Mg and 15% of Si. This would  
327 have left the Mg/Si ratio of the Earth basically unchanged, but would have increased the  
328 Al/Si ratio by 17%. For instance, in Fig. 7 at a value of 0.3 on the x-axis, the Mg/Si  
329 ratio predicted by our model falls in the middle of the observed uncertainty. The Al/Si  
330 ratio predicted by the model is too low (1.2), but with 15% Si evaporation it would have  
331 increased to 1.38, i.e. again in the middle of observed uncertainty. Thus, our model is  
332 consistent with the Al/Si and Mg/Si ratios of the bulk Earth, even if their uncertainties are  
333 correlated, provided that the evaporation of Si and Mg invoked to explain their isotopic  
334 fractionation is taken into account.

335 Second, Alexander (2019) noted a correlation between the depletion of Al and the  
336 depletion of alkali elements in the NCCs. He concluded that alkalis were sequestered in  
337 the refractory material subtracted from these meteorites. Thus, if this material had been  
338 added to the Earth, our planet would be alkali-rich instead of alkali-poor. Although we  
339 have based our argument only on Na, in Sect. 4 we showed that the removal of a refractory  
340 component makes alkalis much more volatile than expected in an equilibrium condensation.  
341 Thus, the correlation between the depletions of alkalis and Al can be explained without the  
342 sequestration of the alkalis in the refractory material. Consequently, the addition of the  
343 refractory material to the Earth would make our planet alkali-poor, not alkali-rich.

344 Finally, Alexander (2019) noted a correlation between the depletion of Al in the NCCs

345 and the isotopic ratios of some elements, such as Ti and Cr. He concluded that the removed  
346 refractory material carried strong isotopic anomalies for these elements. However, these  
347 anomalies are not observed in the Earth, implying that our planet did not accrete the  
348 refractory material missing from the NCCs. We find (Fig. 6a) that the refractory material  
349 at 1,400 K would have sequestered virtually all of the Ti and, for a sufficiently high C/O  
350 ratio, all the Cr as well. Thus, the observed differences in Ti and Cr isotopic compositions  
351 among the NCCs cannot be related to the condensation and removal of this refractory  
352 material and instead have to be due to the isotopic heterogeneity of the solar-composition  
353 material in the disk, although the origin of this heterogeneity is not well understood.

354 We remark that in the case of  $C/O \geq 0.9$ , the bulk Earth should have a Cr/Si ratio  
355 larger than the CI value (as Cr is captured in the first-formed planetesimals). But Cr  
356 is a moderate siderophile element, so that most of it could be in the Earth’s core (e.g.,  
357 McDonough and Sun, 1995), explaining why the bulk *silicate* Earth is depleted in Cr.

358 We end this discussion by commenting that it is certainly possible to envision that  
359 the refractory material sequestered from the NCCs disappeared without contaminating the  
360 Earth. For instance, refractory elements could be locked-up in grains large enough to be out  
361 of equilibrium with the gas, but still small enough to migrate by gas-drag into the Sun. But  
362 then, one has to invoke that the Earth accreted some other refractory-rich material, that  
363 did not contaminate the NCCs although being isotopically identical to the ECs. Possibly  
364 by lack of imagination, we cannot envision a reasonable scenario for this to have happened.  
365 Thus, we conclude that the addition to the Earth of the refractory material sequestered  
366 from the NCCs remains the best option.

## 6. Conclusions and discussions

### 6.1. Summary of results

In this work, we have proposed an astrophysical scenario, consistent with current models of disk evolution and planetesimal formation, that can explain the sequestration of refractory elements from the source region of the non-carbonaceous (NCC) chondrites and, therefore, their sub-solar Al/Si and Mg/Si ratios.

In brief, while the disk was cooling, the massive condensation of olivine changed the disk from a low-dust to a high-dust environment, quenched the magneto-rotational instability of the disk, triggering the sudden formation of a first generation of planetesimals and the sequestration of the already condensed solid material. That material was, therefore, no longer available for the evolution of the gas-solid equilibrium chemistry. With a further decrease in temperature, new solids could form from residual gas. We called these “residual condensates” and the region where these events happened the “residual condensate region” (RCR). For genetic reasons, the first planetesimals and the residual condensates are complementary relative to the solar (CI) values in terms of Al/Si and Mg/Si ratios.

We envisioned that the NCCs formed from a combination of these residual condensates and material that had solar composition in terms of refractory and moderately volatile elements. This material consisted of local grains that were not incorporated in the first planetesimals and remained at equilibrium with the gas and -possibly- also grains that formed farther out in the disk, and migrated into the RCR without suffering element fractionation.

We have shown that, if the first planetesimals formed at a temperature of  $\sim 1,400$  K, (for a pressure of  $10^{-3}$  bar and solar C/O, and a lower temperature, nevertheless exceeding 1,000 K, for lower pressure and/or increased C/O) the mixture of appropriate proportions of

391 solar-composition grains and residual condensates can reproduce simultaneously the Al/Si  
392 and Mg/Si ratios of all the NCCs. Obviously, the amount of solar-composition material has  
393 to increase from the ECs to OCs, as the latter have compositions that are closer to the CI  
394 ratios. We also explained the correlation between the deficits of Na and Al in the NCCs,  
395 as a result of the fact that the sequestration of Al makes Na much more volatile than in  
396 an equilibrium condensation sequence (see Sect. 4). To explain the correlation between the  
397 deficits of Cr and Al, we had to invoke that the first condensates formed in a gas with  
398  $C/O \geq 0.9$ , in agreement with previous work on the ECs (e.g., Larimer, 1975; Lodders and  
399 Fegley, 1993).

400 We showed that the Al/Si and Mg/Si ratios of the Earth can also be understood if  
401 our planet formed from a mixture of first planetesimals and solar-composition material.  
402 Alexander (2019) explicitly excluded this possibility, but we provided in Sect. 5 some  
403 possible solutions to the obstacles that he discussed for this scenario. Our full scenario is  
404 sketched in Fig. S3, which presents a global view of the composition of the disk as time  
405 evolves.

406 Our model is appealing in that it solves two long-standing problems. First, it explains  
407 the sub-solar Al/Si and Mg/Si ratios of the NCCs within a fractionated condensation  
408 sequence. Second, it clarifies the genetic relationship between the Earth and the ECs, as  
409 discussed below. Nevertheless, our model is simple and should be regarded mostly as a  
410 proof of concept. For instance, we assumed that all first planetesimals formed at the same  
411 temperature, so that all the objects we considered are composed of only two components:  
412 residual condensates and solar-composition material for the NCCs or refractory-rich  
413 planetesimals and solar-composition material for the Earth.

## 6.2. Earth – enstatite chondrites relationship

414

415 As discussed in the introduction, the isotopic compositions of the Earth and of the  
416 ECs in terms of non-mass dependent isotopic variations are extremely similar. No other  
417 known meteorite class approximates the Earth better than the ECs from the isotopic point  
418 of view. But element ratios are so different that it is difficult to envision making the Earth  
419 out of the ECs. Here we find that an important component of the Earth is represented  
420 by the first planetesimals, while an important component of the ECs is represented by  
421 residual condensates. First planetesimals and residual condensates are complementary  
422 in terms of element ratios, but they both form out of the same gas in the RCR, so it  
423 is not surprising that they are isotopically very similar. In some sense, with the first  
424 refractory-rich planetesimals we have identified the hidden reservoir of objects with the same  
425 isotope composition as the ECs but different chemical composition, that was postulated by  
426 Dauphas (2017) to explain the Earth. The opposite mass-dependent isotopic fractionation  
427 of Si in the Earth and ECs may be a natural consequence of the formation of the first  
428 condensates, as discussed by Kadlag et al. (2019).

429

430 Pushed further, the genetic relationship between the Earth and the ECs illustrated  
431 in this paper can also help to understand the small differences in their respective Nd,  
432 Mo and Ru isotopic compositions. The Earth has an endmember isotopic composition  
433 relative to known meteorites, slightly enriched in isotopes produced by the s-process with  
434 respect to the ECs (see Burkhardt et al. 2016 and Bouvier and Boyet, 2016 for Nd;  
435 Burkhardt et al., 2014 for Mo and Fischer-Gödde and Kleine, 2017 for Ru). If, for some  
436 reason, the material that condensed directly in the RCR is enriched in s-process isotopes  
437 relative to the solar-composition grains coming into the RCR once the temperature has  
438 decreased, we can understand this difference. In fact, in this case the first planetesimals  
and the residual condensates would have the same proportion of s-process isotopes but, as

439 shown in Sect. 3.2, the Earth, EC and OC meteorites incorporated increasing fractions of  
440 solar-composition material, thus explaining -at least qualitatively- the relative ranking of  
441 s-process enrichment/deficiency observed in these objects.

### 442 **6.3. Chondrules and CAIs**

443 Although we invoke here the mixing of residual condensates and solar-composition  
444 grains to make the ECs and OCs, these meteorites are made of chondrules and not grains.  
445 Chondrule formation is still not fully understood (Krot et al., 2018) and presumably the  
446 mixing we invoke occurred at the level of chondrule precursors and were transformed in  
447 the high-temperature events that led to chondrule formation. Our elemental and isotopic  
448 considerations should nevertheless hold even in this more complex scenario.

449 The relationship between the first condensed material discussed in this paper and the  
450 refractory materials (CAIs, AOAs) found in mostly in the CCs is more elusive. It would  
451 be tempting to identify CAIs with a fraction of the minerals condensed at  $T \gtrsim 1,500$  K  
452 that escaped incorporation in the first generation of planetesimals and somehow reached  
453 the outer disk. But CAIs also carry isotopic anomalies (for instance in Nd or Mo) related  
454 to the p- and r-processes, which are not observed in the Earth, ECs and OCs. **However,**  
455 **Ebert et al. (2018) claim to have identified a refractory component isotopically**  
456 **distinct from CAIs in OCs. The first condensed material discussed in this paper**  
457 **would rather correspond to this refractory component rather than CAIs.**

### 458 **6.4. Protoplanetary disk properties and grain dynamics**

459 Although our work does not specify where the RCR was located, the fact that the first  
460 planetesimals have to be a primary component of the Earth suggests that the sequence of

461 events described in this paper happened at  $\sim 1$  AU. This implies that the disk at  $\sim 1$  AU  
 462 was originally hotter than 1,400K. Viscous-disk models (Bitsch et al., 2015) suggest that the  
 463 temperature at 1 AU was initially lower, but these models neglect the heat released by the  
 464 accretion of gas from the interstellar medium onto the disk, which was presumably vigorous  
 465 at early times (P. Hannebelle, private communication). So, our model does not seem  
 466 unreasonable, but it points to a disk much more complex than those usually envisioned.

467 **As long as the infall of gas on the inner disk is vigorous, the temperature**  
 468 **remains very high. For instance, Baillié et al. (2018) find a temperature**  
 469 **larger than 1,500 K up to 2 AU from the Sun for the first  $10^5$  y. Thus, in**  
 470 **this timeframe, only the gas viscously spreading beyond 2 AU would cool**  
 471 **and condensate. Then, when the infall wanes, the temperature in the inner**  
 472 **disk starts to decrease and condensation can occur *locally*, producing a second**  
 473 **condensation front moving towards the star. The fractional condensation**  
 474 **discussed in this paper would correspond to this second condensation front.**  
 475 **This view of two condensation fronts could explain the difference between CAIs**  
 476 **and the non-CAI refractory component of Ebert et al. (2018), if the isotopic**  
 477 **properties of the infalling gas changed over time, as invoked in Nanne et al.**  
 478 **(2019) to explain the isotopic radial heterogeneity of the protosolar disk<sup>3</sup>.**  
 479 **Similarly, if the gas changed of chemical composition, the high local C/O ratio**  
 480 **required to explain Cr-abundances can be explained as well. Indeed, filaments**  
 481 **of gas are observed to fall onto protoplanetary disks (Alves et al., 2019),**  
 482 **carrying a different C/O composition (Segura-Cox, private communication).**  
 483 **Moreover, the rapid drop of temperature to  $\sim 850$  K followed by slow cooling, that our**

---

<sup>3</sup>see Jacquet, 2019, for a discussion of the possibility that CAIs formed relatively far from the Sun from the point of view of  $^{10}\text{Be}$  production

484 model requires to end the residual condensation before the condensation of Na, could be  
485 due to the transition from a disk dominated by a rapidly waning infall of material from the  
486 ISM to a disk dominated by its own viscous evolution. **Admittedly, this scenario is**  
487 **speculative, but it is not implausible.**

488 Our model also implies that the transition from the MRI-active to the MRI-dead zones  
489 of the disk happened at a temperature between 1,060 and 1,400 K depending on pressure  
490 and C/O ratio, but nevertheless larger than the temperature of condensation of K, whereas  
491 Desch and Turner (2015) argued that the condensation of K is the key to reducing the  
492 ionization of the gas and to quenching the MRI. The temperature  $T_{MRI}$  we obtained was  
493 constrained by the elemental ratios in the NCCs. If the first planetesimals could form only  
494 in a MRI-inactive disk and this requires the condensation of K, we expect that K and  
495 refractory elements should always be correlated, which is not the case for the Earth or the  
496 CCs. A possible solution of this conundrum is that the first planetesimals did not form at  
497 the MRI-active/inactive transition, but in the turbulent disk, by concentrating dust into  
498 vortices.

499 In our model, the residual condensates survive in the disk and mix with solar-  
500 composition grains to form eventually the NCCs. However, the parent bodies of these  
501 meteorites formed relatively late, after about 2-3 My (Sugiura and Fujiya, 2014). How  
502 grains could survive in the disk for so long despite their tendency to migrate towards  
503 the Sun is an open problem that this work does not help to solve. Possible explanations  
504 involve turbulent diffusion counteracting radial drift near the midplane of the disk (Ciesla,  
505 2007), reduced or reversed radial drift due to the partial depletion of gas in the inner disk  
506 (Ogihara et al., 2018), recycling of material in disk winds or jets (Ciesla, 2009), lock-up  
507 in planetesimals and later release as collisional droplets (Johnson et al., 2015). We stress  
508 that in our model we do not need that all residual condensates survive. If the total mass

509 of planetesimals with NCC-like compositions was small, only a tiny fraction of residual  
510 condensates may have survived.

511

### 6.5. Closing remarks

512 In summary, up to now the greatly different ratios among major refractory elements in  
513 the Earth and in non-carbonaceous chondrites have challenged our understanding of the  
514 formation of inner Solar System bodies. Although several unknowns remain, we have shown  
515 that the accretion of a first generation of planetesimals during the condensation sequence of  
516 refractory elements and the consequent formation of residual condensates are key processes  
517 that contribute to the solution of this problem.

518

## 7. Acknowledgments

519 We thank K. Burkhardt, T. Kleine, E. Young and N. Dauphas for valuable suggestions  
520 on an earlier version of this manuscript. We thank in particular C. Alexander for an open  
521 discussion on our respective models and B. Fegley and K. Lodders for an in depth critical  
522 assessment of our results during their visit to Nice and their historical perspective on this  
523 long-studied subject. The reviews from two anonymous referees have also helped to improve  
524 the manuscript and clarify the results.

525

## 8. References

- 526 – Alexander, C. M. O’D., Grossman, J. N., Ebel, D. S., Ciesla, F. J. 2008. The  
527 Formation Conditions of Chondrules and Chondrites. *Science* 320, 1617.
- 528 – Alexander, C. M. O’D. 2019. Quantitative models for the elemental and isotopic

- 529 fractionations in the chondrites: The non-carbonaceous chondrites. *Geochimica et*  
530 *Cosmochimica Acta* 254, 246.
- 531 – Alves, F. O., and 6 colleagues 2019. Gas flow and accretion via spiral streamers and  
532 circumstellar disks in a young binary protostar. *Science* 366, 90.
- 533 – Baillié, K., Marques, J., Piau, L. 2019. Building protoplanetary disks from the  
534 molecular cloud: redefining the disk timeline. *Astronomy and Astrophysics* 624, A93.
- 535 – Bale, C. W., et al., 2016. FactSage Thermochemical Software and Databases,  
536 2010-2016, *Calphad*, vol. 54, pp 35-53, 2016
- 537 – Ballmer, M. D., Houser, C., Hernlund, J. W., Wentzcovitch, R. M., Hirose, K. 2017.  
538 Persistence of strong silica-enriched domains in the Earth’s lower mantle. *Nature*  
539 *Geoscience* 10, 236.
- 540 – Barshay, S. S., Lewis, J. S. 1976. Chemistry of primitive solar material.. *Annual*  
541 *Review of Astronomy and Astrophysics* 14, 81.
- 542 – Bitsch, B., et al. 2015. The structure of protoplanetary discs around evolving young  
543 stars. *Astron. Astrophys.* 575, A28.
- 544 – Bouvier, A., Boyet, M., 2016. Primitive Solar System materials and Earth share a  
545 common initial  $^{142}\text{Nd}$  abundance. *Nature* 537, 399-402.
- 546 – Burkhardt, C., et al., 2014. Evidence for Mo isotope fractionation in the solar nebula  
547 and during planetary differentiation. *Earth Planet. Sci. Lett.* 391, 201-211.
- 548 – Burkhardt, C., et al., 2016. A nucleosynthetic origin for the Earth’s anomalous  $^{142}\text{Nd}$   
549 composition. *Nature* 537, 394-398.
- 550 – Ciesla, F. J., 2007. Outward Transport of High-Temperature Materials Around the  
551 Midplane of the Solar Nebula. *Science* 318, 613.

- 552 – Ciesla, F. J., 2009. Dynamics of high-temperature materials delivered by jets to the  
553 outer solar nebula. *Met. Pl. Sci.* 44, 1663-1673.
- 554 – Dauphas, N., Poitrasson, F., Burkhardt, C., Kobayashi, H., Kurosawa, K. 2015.  
555 Planetary and meteoritic Mg/Si and  $\delta^{30}\text{Si}$  variations inherited from solar nebula  
556 chemistry. *Earth and Planetary Science Letters* 427, 236.
- 557 – Dauphas, N., 2017. The isotopic nature of the Earth's accreting material through  
558 time. *Nature* 541, 521-524.
- 559 – Desch, S. J., Turner, N. J. 2015. High-temperature Ionization in Protoplanetary Disks.  
560 *The Astrophysical Journal* 811, 156.
- 561 – Ebel D. S, 2006. Condensation of Rocky Material in Astrophysical Environments.  
562 In: *Meteorites and the Early Solar System II*, D. S. Lauretta and H. Y. McSween Jr.  
563 (eds.), University of Arizona Press, Tucson, 943 pp., p.253-277.
- 564 – Ebel D. S and Grossman L., 2000. Condensation in dust-enriched systems. *Geochim.*  
565 *Cosmochim. Acta*, 64, 339-366.
- 566 – Ebert, S., et al., 2018. Ti isotopic evidence for a non-CAI refractory component in the  
567 inner Solar System. *Earth Planet. Sci. Lett.* 498, 257-265.
- 568 – Eriksson, G, Hack, K., 1990. ChemSage - A computer program for the calculation of  
569 complex chemical equilibria, *Metall. Trans. B*, 21B, 1013
- 570 – Fegley, B., Lewis, J. S. 1980. Volatile element chemistry in the solar nebula: Na, K,  
571 F, Cl, Br, and P. *Icarus* 41, 439.
- 572 – Fischer-Gödde, M., Kleine, T., 2017. Ruthenium isotopic evidence for an inner Solar  
573 System origin of the late veneer. *Nature* 541, 525-527.

- 574 – Flock, M., Fromang, S., Turner, N. J., Benisty, M. 2017. 3D Radiation Nonideal  
575 Magnetohydrodynamical Simulations of the Inner Rim in Protoplanetary Disks. *The*  
576 *Astrophysical Journal* 835, 230.
- 577 – Güttler, C., et al., 2010. The outcome of protoplanetary dust growth: pebbles,  
578 boulders, or planetesimals?. I. Mapping the zoo of laboratory collision experiments.  
579 *Astron. Astrophys.* 513, A56.
- 580 – Hezel, D. C., et al., 2008. Modal abundances of CAIs: Implications for bulk chondrite  
581 element abundances and fractionations. *Met. Pl. Sci.* 43, 1879-1894.
- 582 – Holzapfel, C., et al., 2003. Pressure effect on Fe-Mg interdiffusion in  $(\text{Fe}_x\text{Mg}_{1-x})\text{O}$ ,  
583 ferropericlase. *Phys. Earth Planet. Int.* 139, 21-34.
- 584 – Hyung, E., Huang, S., Petaev, M. I., Jacobsen, S. B. 2016. Is the mantle chemically  
585 stratified? Insights from sound velocity modeling and isotope evolution of an early  
586 magma ocean. *Earth and Planetary Science Letters* 440, 158.
- 587 – Jacquet, E. 2019. Beryllium-10 production in gaseous protoplanetary disks and  
588 implications for the astrophysical setting of refractory inclusions. *Astronomy and*  
589 *Astrophysics* 624, A131.
- 590 – Javoy, M., 1995. The integral enstatite chondrite model of the Earth. *Geophys. Res.*  
591 *Lett.* 22, 2219-2222.
- 592 – Johansen, A., Youdin, A. 2007. Protoplanetary Disk Turbulence Driven by the  
593 Streaming Instability: Nonlinear Saturation and Particle Concentration. *The*  
594 *Astrophysical Journal* 662, 627.
- 595 – Johnson, B. C., Minton, D. A., Melosh, H. J., Zuber, M. T. 2015. Impact jetting as  
596 the origin of chondrules. *Nature* 517, 339.

- 597 – Kadlag, Y., Tatzel, M., Frick, D. A., Becker, H. 2019. The origin of unequilibrated EH  
598 chondrites - Constraints from in situ analysis of Si isotopes, major and trace elements  
599 in silicates and metal. *Geochimica et Cosmochimica Acta* 267, 300.
- 600 – Krot, A.N., Connolly, H.C., Russel, S. 2018. *Chondrules : records of protoplanetary*  
601 *disk processes*. Cambridge University Press.
- 602 – Larimer, J. W. 1975. The effect of C/O ratio on the condensation of planetary  
603 material. *Geochim. Cosmochim. Acta* 39, 389-392.
- 604 – Larimer, J. W. 1979. The condensation and fractionation of refractory lithophile  
605 elements. *Icarus* 40, 446.
- 606 – Lodders, K., Fegley, B. 1993. Lanthanide and actinide chemistry at high C/O ratios  
607 in the solar nebula. *Earth and Planetary Science Letters* 117, 125.
- 608 – Lodders, K. 2000. An Oxygen Isotope Mixing Model for the Accretion and  
609 Composition of Rocky Planets. *Space Science Reviews* 92, 341.
- 610 – McDonough, W.F. and Sun, S.-s., 1995. The composition of the Earth. *Chem Geol*  
611 120, 223-253.
- 612 – Morbidelli, A., et al., 2016. Fossilized condensation lines in the Solar System  
613 protoplanetary disk. *Icarus* 267, 368-376.
- 614 – Mysen, B. O., Kushiro, I. 1988. Condensation, evaporation, melting, and crystallization  
615 in the primitive solar nebula: experimental data in the system MgO-SiO-H<sub>2</sub> to  
616 1.0x10<sup>-9</sup>bar and 1870C with variable oxygen fugacity.. *American Mineralogist* 73, 1.
- 617 – Nanne, J. A. M., Nimmo, F., Cuzzi, J. N., Kleine, T. 2019. Origin of the non-  
618 carbonaceous-carbonaceous meteorite dichotomy. *Earth and Planetary Science Letters*  
619 511, 44.

- 620 – Ogiwara, M., et al., 2018. Formation of the terrestrial planets in the solar system  
621 around 1 au via radial concentration of planetesimals. *Astron. Astrophys.* 612, L5.
- 622 – Palme, H. and O'Neill, H. St. C., 2014. Cosmochemical estimates of mantle  
623 composition. *Treatise on Geophysics Vol. 3.* Elsevier pp. 1-39.
- 624 – Pringle, E.A., Moynier, F., Savage, P.S., Badro, J. and Barrat, J.A., 2014. Silicon  
625 isotopes in angrites and volatile loss in planetesimals. *PNAS*, 48, 17029-17032
- 626 – Rubie, D.C., Nimmo, F., Melosh, H.J. 2015. Formation of the Earth's Core. In:  
627 *Treatise on Geophysics Vol. 9* Elsevier pp. 43-79.
- 628 – Sugiura, N., Fujiya, W. 2014. Correlated accretion ages and  $\epsilon^{54}\text{Cr}$  of meteorite parent  
629 bodies and the evolution of the solar nebula. *Meteoritics and Planetary Science* 49,  
630 772.
- 631 – Yang, C.-C., et al., 2017. Concentrating small particles in protoplanetary disks  
632 through the streaming instability. *Astron. Astroph.* 606, A80.
- 633 – Yoneda, S., Grossman, L., 1995. Condensation of CaO sbnd MgO sbnd Al<sub>2</sub>O<sub>3</sub>sbnd  
634 SiO<sub>2</sub> liquids from cosmic gases. *Geochim. Cosmochim. Acta* 59, 3413-3444.
- 635 – Youdin, A. N., Goodman, J., 2005. Streaming Instabilities in Protoplanetary Disks.  
636 *Astron. J.* 620, 459-469.
- 637 – Young, E., et al., J., 2019. Near-equilibrium isotope fractionation during planetesimal  
638 evaporation. *Icarus*, 323, 1.